



Synthesis of three dimensional extended conjugated polyimide and application as sodium-ion battery anode



Zhongtao Li^a, Jingyan Zhou^a, Rongfei Xu^a, Shuiping Liu^b, Yuankun Wang^a, Peng Li^a, Wenting Wu^{a,*}, Mingbo Wu^{a,*}

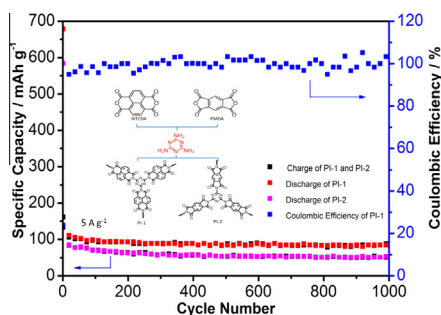
^aState Key Laboratory of Heavy Oil Processing, China University of Petroleum, Qingdao 266580, China

^bState Key Laboratory for Modification of Chemical Fibers and Polymer Materials, Donghua University, Shanghai 201620, China

HIGHLIGHTS

- Three dimensional extended conjugated polyimides have been facilely prepared.
- The capacitance of obtained polymer is 88.8 mAh g⁻¹ after 1000 cycles at 5.0 A g⁻¹.
- Synergistic effect exists in electron withdrawing amide groups and triazine rings.
- As-made polyimide is a promising candidate for Na-ion battery anode.

GRAPHICAL ABSTRACT



ARTICLE INFO

Article history:

Received 5 August 2015

Received in revised form 19 November 2015

Accepted 20 November 2015

Available online 23 November 2015

Keywords:

Polyimide

Sodium-ion battery

Anode

Electrochemical performance

ABSTRACT

Two covalent polyimides with different conjugated subunits have been synthesized as sodium-ion batteries anode. The melamine and two commercially available dianhydrides have been adopted as building blocks to fabricate 3D extended covalent frameworks, which are consisted of electron withdrawing amide groups and triazine rings to coordination with Na ions. The results revealed that cross-linked polymer exhibits excellent durability and rate capacity (88.8 mAh g⁻¹ at a current density of 5.0 A g⁻¹ after 1000 cycles), which provides a promising candidate for high performance Na-ion battery anode.

© 2015 Elsevier B.V. All rights reserved.

1. Introduction

Lithium-ion batteries (LIBs) are considered to be promising candidates of energy-conversion and energy-storage systems because of their high energy density, long cycling life in the past two decades [1–4]. However, the use of lithium is hampered by cost restriction and the resources of lithium would run out in future. Recently, increasing attentions are turning to Na-ion batteries (NIBs) as low-cost alternative technology other than LIBs. The

abundance in the earth and low cost of Na become great advantageous when large amount of electrode materials are demanded for energy storage [5]. Furthermore, NIBs can utilize inexpensive aluminum current collectors for anodes because Al does not alloy with Na, whereas LIBs have to use expensive copper [6–8].

Currently, there has been great fascinating in developing advanced electrode materials for NIBs, and a large number of materials involving transition metal oxides have been proposed as cathodes, similar to those explored for LIBs [9–12]. Cao et al. reported a fabrication of single crystalline Na₄Mn₉O₁₈ nanowires with a high reversible capacity (128 mAh g⁻¹ at 0.1 C, 1 C corresponds to 120 mA g⁻¹) and exceptional cycling performance as NIBs cathode

* Corresponding authors.

E-mail addresses: wuwt@upc.edu.cn (W. Wu), wumb@upc.edu.cn (M. Wu).

[11]. Yang and co-workers synthesized a $\text{Na}_4\text{Fe}(\text{CN})_6/\text{C}$ nanocomposite with exceptional cycling stability and high rate capability as NIBs cathode [12]. However, with regard to anodes, the commercial LIBs anode, i.e. graphitic carbon, does not perform well in NIBs due to its terrible capacity (31 mAh g^{-1}) [8]. The reason is that the Na-ion is larger than Li-ion (diameter: 2.32 vs 1.80 \AA), which may increase the difficulty of insertion/extraction into the conjugated layers of graphitic during cycling [13]. Built upon the success of LIBs, intercalation-type inorganic anodes have been investigated for NIBs, where the performance is typically inferior than their LIBs counterparts due to the larger size of Na ions and the associated more dramatic and frequent structural changes during electrochemical cycling [14]. Meanwhile, covalent organic materials, owing to their abundance, design flexibility and environmental benignancy, especially the flexibility of structure facilitate the higher mobility of large-sized sodium ions, have lately enjoyed a renewed interest as electrodes in rechargeable sodium batteries [15].

Remarkably, organic carbonyl compounds are considered to be prospective electrode materials for NIBs due to their distinguish advantages, including lightweight, redox stability, multi-electron reactions, and availability from easily accessible natural sources [16]. Recently, coordination compounds 4,4'-Biphenyldicarboxylate sodium as anodes for Na-ion batteries elucidated the correlation between the structural properties of organic anodes and their electrochemical performances (200 mAh g^{-1} , 20 mA g^{-1}) have been investigated by Kyu Tae Lee and co-workers [17]. Xia and co-workers [18] reported a polyimide just delivers a reversible capacity of 140 mAh g^{-1} at the rate of 1 C (140 mA g^{-1}) and 84 mAh g^{-1} at the rate of 30 C (2520 mA g^{-1}). Zhang and co-workers demonstrated the use of aromatic carbonyl derivatives polyimides as cathode materials for NIBs (135.7 mAh g^{-1} , 24 mA g^{-1}) for the first time, which lays the foundation for future researches [19]. However, most of them were tested in a slow charge/discharge process (e.g. 20 mA g^{-1} , which takes a very long time for a charge/discharge) [7–9], and those tested under fast charge/discharge process often led to significant performance degradation. This phenomenon maybe ascribed to the poor conductivity of molecules and dissolve of the active material into electrolytes during cycling [9,19,20].

Herein, we utilize two commercially available dianhydrides (Fig. 1) namely pyromellitic dianhydride (PMDA) and naphtha-

lene-1,4,5,8-tetracarboxylic dianhydride (NTCDA) as building blocks to polymerize with melamine for fabricating dianhydride-based polyimides (PIs). The electron withdrawing amides and triazine rings in the monomers could coordinate with Na ions to increase the storage capability. The amino-groups of melamine located on three directions could effectively build up 3D expanded cross-linked network. After solution treatment, the active oligomers polymerized in depth at high temperature to constructed highly stable and conjugated framework, which could provide an effectively path to overcome these problems that mentioned above. With the improvement on the electrochemical stability and electronic conductivity, these materials could afford more reactive sites for electrode–electrolyte interaction and accelerate electron and ion transportation during reversible sodiation/desodiation processes. The electrochemical experiment data revealed that a high capacity, stable cycling life and ultrafast rechargeable anode for NIBs has been obtained.

2. Experimental

2.1. Materials preparation

All chemicals were commercially available grade and used without further purification. All of the solvents were dried by 4A molecular sieve before use.

2.2. Preparation of PI-1 and PI-2

A mixture of melamine (10 mmol) and dianhydride (NTCDA or PMDA) (15 mmol) were refluxed in N,N-Dimethylformamide (DMF, 30 mL) for 15 h under Ar protection at $150 \text{ }^\circ\text{C}$. After reaction, the precipitates were filtrated and washed with ethanol for three times then dried at $75 \text{ }^\circ\text{C}$ in vacuum oven for 5 h. Then, the oligomers were heated at $330 \text{ }^\circ\text{C}$ in nitrogen for 6 h. Finally, the solid was washed by acetone twice and water ($60 \text{ }^\circ\text{C}$) twice to obtain the final products. The polyimide that prepared from NTCDA and PMDA is labeled as PI-1 and PI-2, respectively.

2.3. Analysis instruments

The chemical structures of the samples were characterized by Fourier transform infrared spectrometry (FTIR, Thermo Nicolet NEXUS 670, USA). X-ray photoelectron spectroscopy (XPS, Thermo Scientific ESCALab250Xi, Al $K\alpha$) was used to characterize chemical structure in further. The XRD pattern of the polyimides was recorded on an X'Pert PRO MPD X-ray diffractometer equipped with a monochromatized Cu $K\alpha$ radiation from 10° to 75° . The stabilization of monomer and polymer were determined by thermogravimetric analysis (TGA, Netzsch STA 449C, Germany).

2.4. Electrochemical measurement

Working electrodes were prepared by mixing 50 wt% active materials, 30 wt% carbon black and 20 wt% binder in N-methyl-2-pyrrolidinone (NMP) for 20 min grinding in a mortar to form homogeneous slurry, which was then coated onto an aluminum foil current. The prepared working electrode was dried at $120 \text{ }^\circ\text{C}$ under vacuum for 8 h to remove the solvent before fabrication. Finally, the electrodes were cut into disks, and CR2032 cells were assembled in an argon-filled glove box with sodium metal foil as counter and reference electrode, Glass microfiber filters (GF/D) as separator, and 1 M NaClO_4 in ethylene carbonate and diethyl carbonate (EC/DEC, 1:1 v/v) as electrolyte. Galvanostatic charge–discharge cycles were conducted on a LAND CT2001A battery tester at different current densities in the voltage range from 0.05 V to 2.5 V . The cyclic

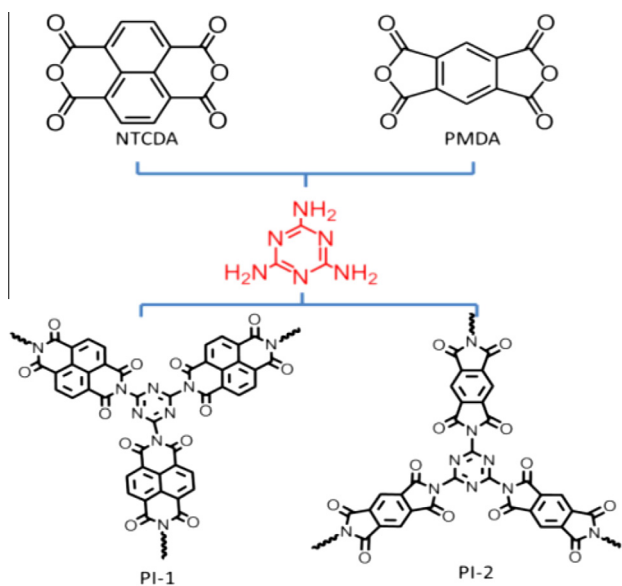


Fig. 1. Synthetic pathway of the polyimides.

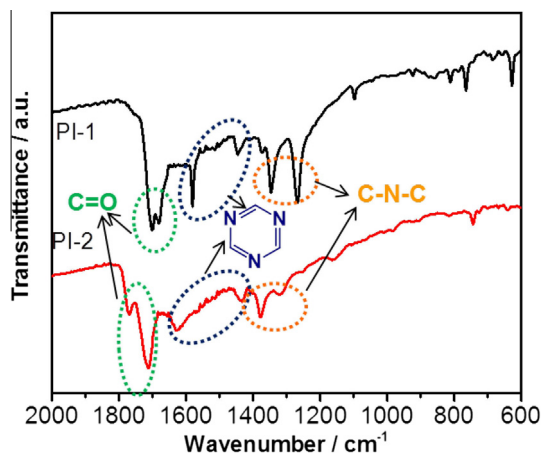


Fig. 2. FT-IR spectra of polymer PI-1 and PI-2.

voltammetry was measured by using an Ametek PARSTAT4000 electrochemistry workstation between 0.05 V and 2.5 V (vs Na/Na⁺) at a constant scanning rate of 0.2 mV s⁻¹. Electrochemical impedance spectroscopy (EIS) studies were carried out on the same electrochemistry workstation by applying a perturbation voltage of 10 mV in a frequency range of 100 kHz–10 mHz.

3. Results and discussion

3.1. Structural characterization of polyimides

In order to research the molecular structure of the cross-linked polyimide, Fourier transform infrared (FT-IR) spectra, X-ray

photoelectron spectroscopy (XPS) of the materials were examined. FT-IR spectra of PI-1 and PI-2 are shown in Fig. 2. Both two polymers exhibit similar absorption peaks, which reflect the comparable functional groups. The absorptions at 1703, 1677.5 cm⁻¹ (PI-1) and 1773, 1714.6 cm⁻¹ (PI-2) were ascribed to the stretching vibrations of asymmetric stretching and symmetric stretching of C=O. Compared with corresponding anhydride monomer, the slightly hypochromatic shift would due to the electro-donating property of imide groups [21]. The absorption bands at 1580.9, 1447.6 cm⁻¹ (PI-1) and 1625.48, 1432.8 cm⁻¹ (PI-2) ascribe to triazine ring, indicate the melamine units on polymer backbone [22,23]. The absorption bands at 1580.9 cm⁻¹ (PI-1) and 1625.5 cm⁻¹ (PI-2) also may refer to the aromatic C=C. As shown in Fig. 1, the amino-groups of melamine located on three directions could effectively build up 3D expanded cross-linked network. Two well defined bands at around 1374 cm⁻¹ (PI-1) and 1378 cm⁻¹ (PI-2) are assigned to the stretching vibration of C–N–C, which represent formation of the imide structure in polyimide after thermal treatment at 330 °C.

As shown in XPS spectrums in Fig. 3, both spectrum of the PI-1 and PI-2 possess three peaks centered at 284.8 eV, 399.6 eV and 531.7 eV, corresponding to C 1s, N 1s and O 1s, respectively. The XPS spectrum of the C 1s can be divided into three peaks, centered at 284.8, 286.4 and 288.3 eV. The major C peaks at 284.8 eV correspond to graphitic carbon (sp² carbon), which indicate high degree of conjugated system in these materials. The weak peaks at 286.4 eV and 288.3 eV is identified as C–N single bond or C=O and sp²-bonded carbon (N–C=N) respectively [24], which represented the successful introduction of amides groups and triazine rings into the system. The N 1s spectrum shows two deconvoluted peaks at 398.6 eV and 399.8 eV, which could be assigned to sp²

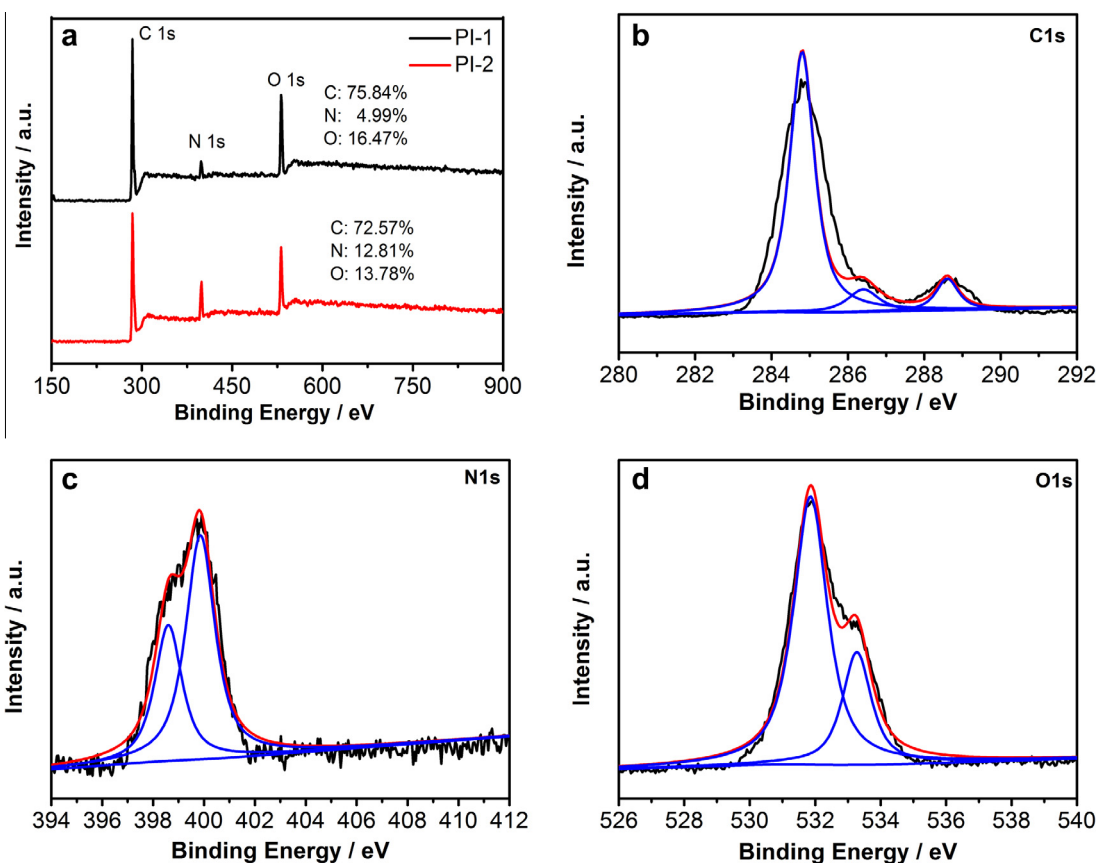


Fig. 3. XPS spectra of PI-1 and PI-2 (a), the C 1s (b), the N 1s (c), and the O 1s (d).

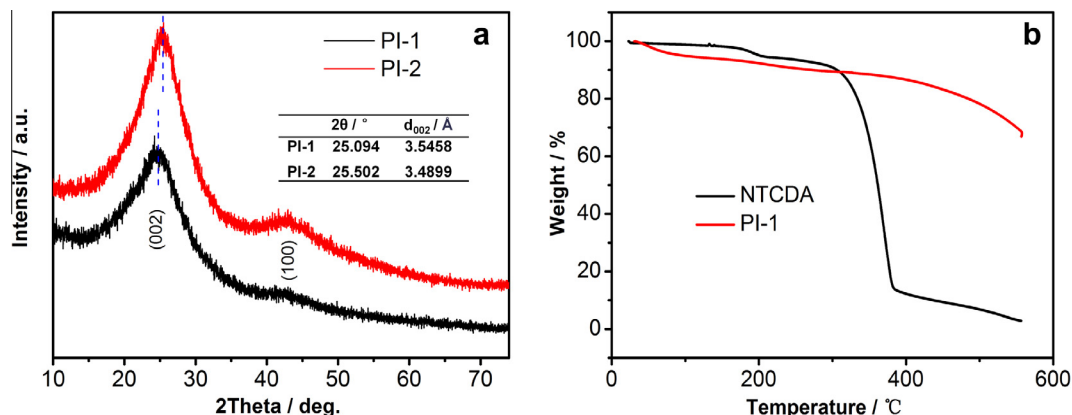


Fig. 4. (a) XRD patterns of PI-1 and PI-2, (b) TGA curves of PI-1 and NTCDA under nitrogen.

hybridized aromatic bonds with carbon (C=N–C) and the single bond with carbon (N–C), respectively. The deconvoluted peaks (Fig. 3d) of O 1s spectrum were resolved into two components at 531.9 eV and 533.2 eV, that can be assigned to C=O band in carbonyl group. The XPS patterns that mentioned above demonstrated the formation of polyimides back bones with the subunits of triazine rings.

As shown in XRD patterns in Fig. 4a, the two polyimides show similar diffraction features and exhibit two broad diffraction peaks (2θ) at around 25.2° and 43.7° , which are similar as the (002) and (100) planes of graphite, respectively [25]. Thereafter, the (002) diffraction peaks (2θ) in PI-1 is somewhat smaller than that of PI-2, which revealed the interplanar spacing of the (002) plane (d_{002}) of PI-1 is larger than PI-2. The naphthalene in PI-1 is larger than benzene in PI-2, which bring some difficulties on interlayer conjugated units array to close with each other. The increase of the d_{002} is beneficial for the Na^+ intercalation and deintercalation [8]. Meanwhile, the movements of larger conjugated systems of PI-1 become harder, which lead to more random arrangement and weaken the (002) diffraction peak. As the result, the random arranged conjugated systems could afford more coordination sites for sodium and increase the capacity as NIBs anode. To assess the thermal properties and the compositions of PI-1, thermogravimetric analysis (TGA) was carried out under nitrogen (Fig. 4b), compared with a rapid mass loss of NTCDA at around 320°C , after the evaporation of absorbed water and solvents below 150°C , PI-1 shows excellent thermal stability until 400°C . The accelerated weight loss that starting at 400°C would be due to the hydrocracking of hydrocarbons.

3.2. Electrochemical characterization of polyimides

As shown in Fig. 5a, the cycling performances as NIBs anode at current density of 500 mA g^{-1} are compared between two materials. PI-1 exhibits higher energy storage capability with a high initial capacity of 1161.2 mAh g^{-1} and good durability, which remains 72.4% (176.7 mAh g^{-1}) capacity of 10th cycle (244.2 mAh g^{-1}) even after cycled 100 times. Meanwhile capacity of PI-2 is just kept at 95.1 mAh g^{-1} after 100 cycles. The larger conjugate naphthalene units in PI-1 seems can help to form highly stable and conductive network, which can increase durability and electron transfer capability [13]. From a theoretical view, lower LUMO energy means better electron affinity (EA) and oxidizability. Correspondingly, higher HOMO energy means lower ionization potential (IP) and better reducibility. Beyond that, the narrow LUMO–HOMO gap (E_g) is related to good electronic conductivity [26,27]. Andrzejak et al. [28] calculated a series EA and IP values of dianhydrides by a DFT method. The EA value of NTCDA units in PI-1 is larger than PMDA units in PI-2, whereas the IP value and E_g value is smaller than that in PI-2, which lead to a higher redox activity and electronic conduction of PI-1 and improved PI-1 electrochemical performance in further.

Rate capability is another important factor to value electrode materials in practical application. The discharge–charge capacity of PI-1 and PI-2 cycled at different current density that varied from 100 mA g^{-1} to 5.0 A g^{-1} are shown in Fig. 5b. The specific capacity of PI-1 at 100 mAh g^{-1} current density after 20 cycles can remain at 330.8 mAh g^{-1} . Significantly, even at a high current density of 5.0 A g^{-1} , the capacity can still keep at 102.3 mAh g^{-1} . Moreover,

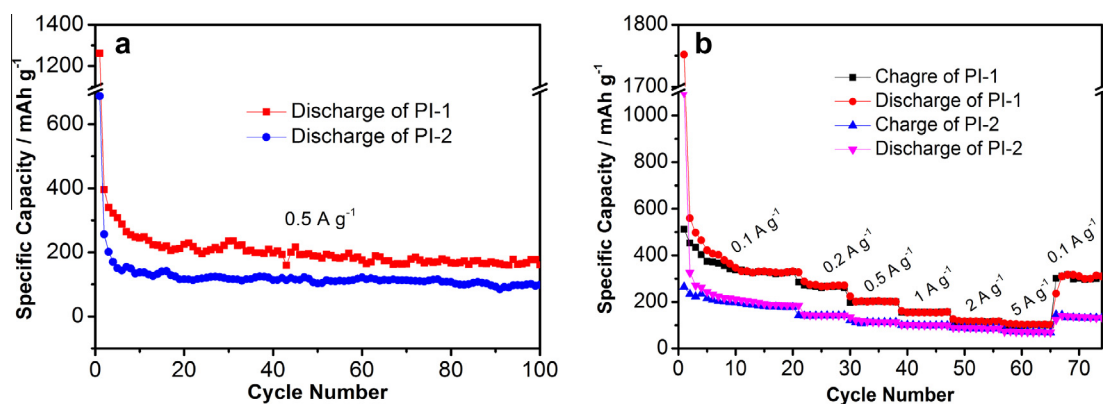


Fig. 5. (a) Cyclic performance of PI-1 and PI-2 electrodes at a current density of 500 mA g^{-1} , (b) rate capacity of PI-1 and PI-2 at various current densities.

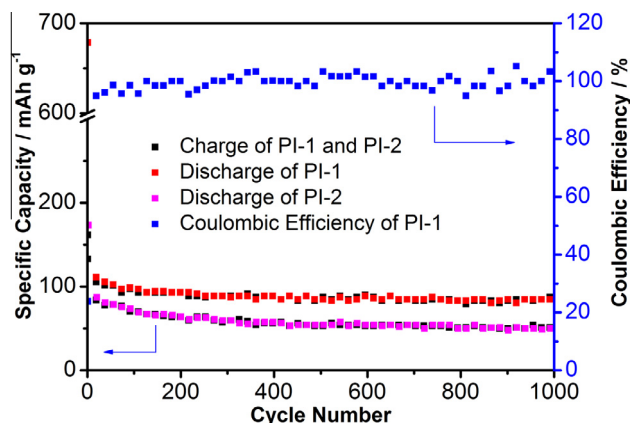


Fig. 6. Long-term cycling performance of PI-1 and PI-2 at 5 A g^{-1} .

the specific capacity rebounds back to 309.9 mAh g^{-1} when the current density turns back to 100 mA g^{-1} after cycled at various current densities, which indicated excellent rate capability and stability of PI-1 electrode. However, PI-2 exhibits inferior specific capacity (69.4 mAh g^{-1} , 5 A g^{-1}) and rate capability ($137.02 \text{ mAh g}^{-1}$, turns back to 100 mA g^{-1}) compared with PI-1. The remarkably capacity and rate capability of PI-1 during cycling is attributed to the good compatibility with electrolyte, high conductivity network and electrochemical stability after cycling.

Fig. 6 shows the long-term cycling stability of PI-1 and PI-2 and the coulombic efficiency of PI-1 at a current density of 5 A g^{-1} . The capacity attenuates in the first 30 cycles due to the irreversible reactions and the formation of SEI film, and then the capacity and coulombic efficiency keeps stable (c.a. 106.9 mAh g^{-1} and 100%, respectively). After 1000 cycles, there is no obvious capacity

decay. The reversible discharge capacity of PI-1 electrodes was retained at 88.8 mAh g^{-1} after 1000 cycles, which is 83.1% of capacity retention compared with the stabilized capacity after 30 cycles. However, PI-2 shows lower capacity (81.9 mAh g^{-1} , 30th cycle) with fast capacity decay (51.1 mAh g^{-1} , 1000th cycle).

Cyclic voltammetry (CV) measurements of PI-1 and PI-2 electrodes were performed in the range of 0.05–2.5 V at a scan rate of 0.2 mV s^{-1} (Fig. 7a and c). The voltage versus capacity profiles of the starting four cycles were carried out at a current density of 100 mA g^{-1} in the voltage window 0.05–2.5 V (vs Na) at room temperature (Fig. 7b and d). As shown in Fig. 7a, a reduction peak at 1.76 V of PI-1 represent the insertion of Na ions into NTCDA and forms sodium enolate $\text{Na}_2\text{PI-1}$. Reduction peak at 1.0 V in the CV curves ($\sim 1.0 \text{ V}$ in Fig. 7b) suggests the incorporation of the other two Na ions into NTCDA to form sodium enolate group and six Na ions into triazine ring coordination with nitrogen finally form $\text{Na}_{10}\text{PI-1}$ [13,29–31]. In addition, the reduction peaks of PI-1 ($\sim 1.0 \text{ V}$) is about 0.1 V higher than that of PI-2 ($\sim 0.9 \text{ V}$). The larger conjugated system and high electron cloud density of naphthalene units would weak the electronic accepting capability of polymer PI-1, which leads to a higher reduction potential. The reduction peak of PI-2 ($\sim 0.9 \text{ V}$) is broader and lower than that of PI-1, which revealed the higher electronic conduction of PI-1 than PI-2 that could accelerate redox process during CV scanning [27]. The two peaks could also be observed in the other three cycles, which demonstrates these oxidation–reduction process are highly reversible. The peak at 0.40 V (starting at 0.6 V in Fig. 7b) in the first reduction process disappears in the subsequent cycles, which can be attributed to irreversible reaction of NTCDA with sodium and the formation of solid electrolyte interphase (SEI) [16,18,32]. In the voltage–capacity profiles of both PI-1 and PI-2, the position of the voltage plateau is consistent with the CV curves. As shown in Fig. 7b, PI-1 has an initial specific capacity of $1751.8 \text{ mAh g}^{-1}$,

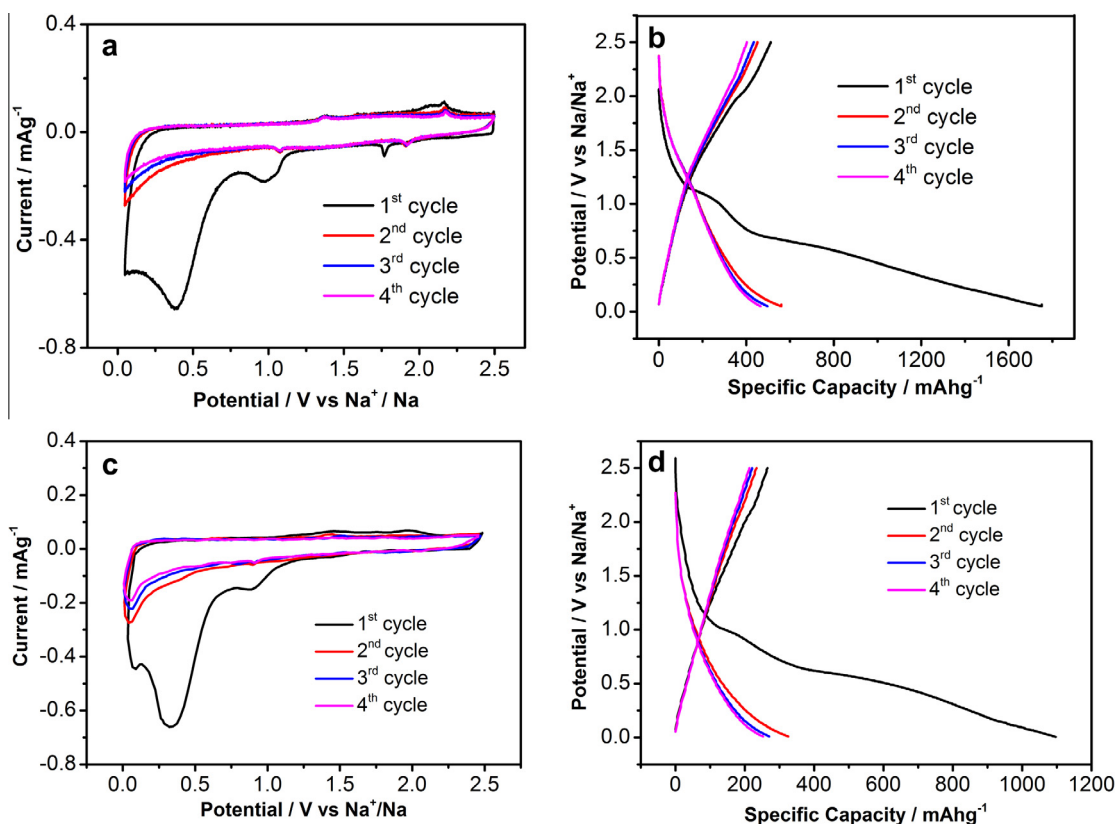


Fig. 7. (a, c) CV curves of PI-1 and PI-2 anodes at 0.2 mV s^{-1} of scanning rate, (b, d) discharge–charge profiles of PI-1 and PI-2 at a constant current density of 100 mA g^{-1} .

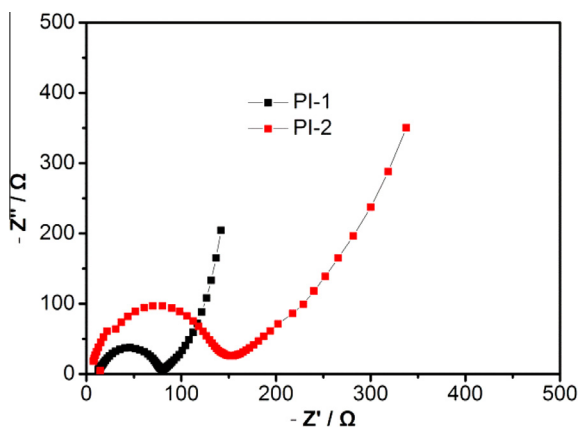


Fig. 8. Nyquist plots of the PI-1 and PI-2 electrodes.

which decrease to 558.9 mAh g^{-1} in the second cycle. Besides, the initial coulombic efficiency recovered to 89% in the second cycle, which is ascribed to the irreversible Na ions insertion and the formation of SEI film.

The electrochemical impedance spectroscopy (EIS) results for PI-1 and PI-2 are shown in the form of Nyquist plots in Fig. 8. Both EIS spectra show a straight line at the low frequency region, which represents the diffusion resistance of sodium. All of them show a semicircle at the high-to-medium frequency region, representing the charge transfer resistance. It should be noted that the diameter of the semicircle for the PI-1 electrodes (80 ohm) is smaller than that of PI-2 (151 ohm), which revealed that the charge transfer resistance of the PI-1 electrode is lower than that of PI-2 electrode. In the low frequency region, PI-1 showed a straight line that is close to the vertical axis, which indicates that the diffusion resistance is lower than PI-2. Both the lower charge transfer resistance and diffusion resistance of PI-1 ascribe to the fabrication of highly conductive network and good compatibility with electrolyte to increase electron transfer capability, which in accordance with the excellent cycling properties and rate capability [33,34].

4. Conclusion

Herein, two covalent polyimides have been synthesized from pyromellitic dianhydride or naphthalene dianhydride and melamine via polymerization. The electronic withdrawing groups (dianhydride and triazine) in obtained polymers can greatly increase Na-ions storage capability. The three aminos of melamine located on different directions can effectively fabricate three-dimensional expanded conjugated network, which afford excellent durability and rate capacity as electrode in NIBs. The capacity of PI-1 could be maintained 176.6 mAh g^{-1} after 100 charge/discharge cycles at the current density of 500 mA g^{-1} . Even at much higher current density of 5 A g^{-1} , a reversible capacity of 88.8 mAh g^{-1} is achieved. The better electrochemical performance of PI-1 would be due to the large conjugated naphthalene as subunits to form higher stable and conductive network. These materials described here would potentially afford a way to develop novel organic anode materials with excellent durability and rate capacity for NIBs.

Acknowledgments

This work is supported by the National Natural Science Foundation of China (51303212, 51303202, 21572269, 21302224, 51372277); National Natural Science Foundation of Shandong Province (ZR2013BQ028, ZR2013EMQ013); The Fundamental

Research Fund for the Central Universities (14CX02196A, 15CX08005A, 15CX05010A) and Open Fund of Beijing National Laboratory for Molecular Sciences (2013019) and Open fund of State Key Laboratory for Modification of Chemical Fibers and Polymer Materials (LK1516).

References

- [1] Y. Liang, Z. Tao, J. Chen, Organic electrode materials for rechargeable lithium batteries, *Adv. Energy Mater.* 2 (2012) 742–769.
- [2] H. Wang, Y. Wang, Y. Li, Y. Wan, Q. Duan, Exceptional electrochemical performance of nitrogen-doped porous carbon for lithium storage, *Carbon* 82 (2015) 116–123.
- [3] Z. Li, Y. Wang, H. Sun, W. Wu, M. Liu, J. Zhou, G. Wu, M. Wu, Synthesis of nanocomposites with carbon-SnO₂ dual-shells on TiO₂ nanotubes and their application in lithium ion batteries, *J. Mater. Chem. A* 3 (2015) 16057–16063.
- [4] Z. Li, G. Wu, D. Liu, W. Wu, B. Jiang, J. Zheng, Y. Li, J. Li, M. Wu, Graphene enhanced carbon-coated tin dioxide nanoparticles for lithium-ion secondary batteries, *J. Mater. Chem. A* 2 (2014) 7471–7477.
- [5] M.D. Slater, D. Kim, E. Lee, C.S. Johnson, Sodium-ion batteries, *Adv. Funct. Mater.* 23 (2013) 947–958.
- [6] Y. Kim, K.-H. Ha, S.M. Oh, K.T. Lee, High-capacity anode materials for sodium-ion batteries, *Chem. Eur. J.* 20 (2014) 11980–11992.
- [7] H. Pan, Y.-S. Hu, L. Chen, Room-temperature stationary sodium-ion batteries for large-scale electric energy storage, *Energy Environ. Sci.* 6 (2013) 2338–2360.
- [8] W. Luo, C. Bommier, Z. Jian, X. Li, R. Carter, S. Vail, Y. Lu, J.-J. Lee, X. Ji, Low-surface-area hard carbon anode for Na-ion batteries via graphene oxide as a dehydration agent, *Appl. Mater. Interfaces* 7 (2015) 2626–2631.
- [9] H. Banda, D. Damien, K. Nagarajan, M. Harharan, M.-M. Shaijumon, A polyimide based all-organic sodium ion battery, *J. Mater. Chem. A* 3 (2015) 10453–10458.
- [10] S. Komaba, N. Yabuuchi, T. Nakayama, A. Ogata, T. Ishikawa, I. Nakai, Study on the reversible electrode reaction of Na_{1-x}Ni_{0.5}Mn_{0.5}O₂ for a rechargeable sodium-ion battery, *Inorg. Chem.* 51 (2012) 6211–6220.
- [11] Y. Cao, L. Xiao, W. Wang, D. Choi, Z. Nie, J. Yu, L.V. Saraf, Z. Yang, J. Liu, Reversible sodium ion insertion in single crystalline manganese oxide nanowires with long cycle life, *Adv. Mater.* 23 (2011) 3155–3160.
- [12] J. Qian, M. Zhou, Y. Cao, X. Ai, H. Yang, Nanosized Na₄Fe(CN)₆/C composite as a low-cost and high-rate cathode material for sodium-ion batteries, *Adv. Energy Mater.* 2 (2012) 410–414.
- [13] C. Wang, Y. Xu, Y. Fang, M. Hou, L. Liang, S. Singh, H. Zhao, A. Schober, Y. Lei, Extended π -conjugated system for fast-charge and -discharge sodium-ion batteries, *J. Am. Chem. Soc.* 137 (2015) 3124–3130.
- [14] B. Farbod, K. Cui, W.P. Kalisvaart, M. Kupsta, B. Zahiri, A. Kohandehghan, E.M. Lotfabad, Z. Li, E.J. Lubber, D. Mitlin, Anodes for sodium ion batteries based on tin germanium antimony alloys, *ACS Nano* 8 (2014) 4415–4429.
- [15] M. Armand, J.M. Tarascon, Building better batteries, *Nature* 451 (2008) 652–656.
- [16] W. Luo, M. Allen, V. Raju, X. Ji, An organic pigment as a high-performance cathode for sodium-ion batteries, *Adv. Energy Mater.* (2014), <http://dx.doi.org/10.1002/aenm.201400554>.
- [17] A. Choi, Y.K. Kim, T.K. Kim, M.-S. Kwon, K.T. Lee, H.R. Moon, 4,4'-Biphenyldicarboxylate sodium coordination compounds as anodes for Na-ion batteries, *J. Mater. Chem. A* 2 (2014) 14986–14993.
- [18] L. Chen, W. Li, Y. Wang, C. Wang, Y. Xia, Polyimide as anode electrode material for rechargeable sodium batteries, *RSC Adv.* 4 (2014) 25369–25373.
- [19] H. Wang, S. Yuan, D. Ma, X. Huang, F. Meng, X. Zhang, Tailored aromatic carbonyl derivative polyimides for high-power and long-cycle sodium-organic batteries, *Adv. Energy Mater.* 4 (2013) 1–7.
- [20] Y. Liang, P. Zhang, S. Yang, Z. Tao, J. Chen, Fused heteroaromatic organic compounds for high-power electrodes of rechargeable lithium batteries, *Adv. Energy Mater.* 3 (2013) 600–605.
- [21] O.K. Farha, A.M. Spokoyny, B.G. Hauser, Y.-S. Bae, S. Samantha, E. Brown, R.Q. Snurr, C.A. Mirkin, J.T. Hupp, Synthesis, properties, and gas separation studies of a robust diimide-based microporous organic polymer, *Chem. Mater.* 21 (2009) 3033–3035.
- [22] S. Xiong, X. Fu, L. Xiang, G. Yu, J. Guan, Z. Wang, Y. Du, X. Xiong, C. Pan, Liquid acid-catalysed fabrication of nanoporous 1,3,5-triazine frameworks with efficient and selective CO₂ uptake, *Polym. Chem.* 5 (2014) 3424–3431.
- [23] P. Kuhn, M. Antonietti, A. Thomas, Porous, covalent triazine-based frameworks prepared by ionothermal synthesis, *Angew. Chem. Int. Ed.* 47 (2008) 3450–3453.
- [24] J. Liu, Y. Liu, N. Liu, Y. Han, X. Zhang, H. Huang, Y. Lifshitz, S.-T. Lee, J. Zhong, Z. Kang, Metal-free efficient photocatalyst for stable visible water splitting via a two electron pathway, *Science* 347 (2015) 970–974.
- [25] Y. Mao, H. Duan, B. Xu, L. Zhang, Y. Hu, C. Zhao, Z. Wang, L. Chen, Y. Yang, Lithium storage in nitrogen-rich mesoporous carbon materials, *Energy Environ. Sci.* 5 (2012) 7950–7955.
- [26] X. Han, G. Qing, J. Sun, T. Sun, How many lithium ions can be inserted onto fused C₆ aromatic ring systems, *Angew. Chem. Int. Ed.* 51 (2012) 5147–5151.
- [27] Z. Song, H. Zhan, Y. Zhou, Polyimides: promising energy-storage materials, *Angew. Chem. Int. Ed.* 49 (2010) 8444–8448.

- [28] M. Andrzejak, G. Mazur, P. Petelenz, Quantum chemical results as input for solid state calculations: charge transfer states in molecular crystals, *J. Mol. Struct.* 527 (2000) 91–102.
- [29] G.M. Veith, L. Aggetti, L.A. Adamczyk, B. Guo, S.S. Brown, X.-G. Sun, A.A. Albert, J.R. Humble, C.E. Barnes, M.J. Bojdys, S. Dai, N. Dudney, Electrochemical and solid-state lithiation of graphitic C₃N₄, *Chem. Mater.* 25 (2013) 503–508.
- [30] Y. Fu, J. Zhu, C. Hu, X. Wu, X. Wang, Covalently coupled hybrid of graphitic carbon nitride with reduced graphene oxide as a superior performance lithium-ion battery anode, *Nanoscale* 6 (2014) 12555–12564.
- [31] S.M. Thomas, B.J. Ana, S. Andrea, C. Furio, R.S. Paul, The use of graphitic carbon nitride based composite anodes for lithium-ion battery applications, *Electroanalysis* 27 (2015) 1–7.
- [32] C.D. Luca, C. Giomini, L. Rampazzo, The multi-step reversible reduction of 1,4,5,8-naphthalene tetracarboxylic acid dianhydride: an electrochemical study, *Electroanal. Chem.* 280 (1990) 145–147.
- [33] P. Sharma, D. Damien, K. Nagarajan, M. Shajjumon, M. Hariharan, Perylene-polyimide-based organic electrode materials for rechargeable lithium batteries, *J. Phys. Chem. Lett.* 4 (2013) 3192–3197.
- [34] M.E. Bhosale, K. Krishnamoorthy, Chemically reduced organic small-molecule-based lithium battery with improved efficiency, *Chem. Mater.* 27 (2015) 2121–2126.